Profiling the structural determinants of aminoketone derivatives as hNET and hDAT reuptake inhibitors by field-based QSAR based on molecular docking

Panpan Wang[*], Chenxi Jing, Pei Yu, Meng Lu, Xiaobo Xu, Qinglan Pei and Fengmei Yan
College of Chemistry and Pharmaceutical Engineering, Huanghuai University, Zhumadian, Henan, China

Abstract.
BACKGROUND: Bupropion, one of the dual norepinephrine and dopamine reuptake inhibitors (NDRIs), is an aminoketone derivative performed effect in improving cognitive function for depression. However, its therapeutic effect is unsatisfactory due to poor clinical response, and there are only few derivatives in pre-clinical settings.
OBJECTIVE: This work attempted to elucidate the essential structural features for the activity and designed a series of novel derivatives with good inhibitive ability, pharmacokinetic and medicinal chemistry properties.
METHODS: The field-based QSAR of aminoketone derivatives of two targets were established based on docking poses, and the essential structural properties for designing novel compounds were supplied by comparing contour maps.
RESULTS: The selected two models performed good predictability and reliability with R^2 of 0.8479 and 0.8040 for training set, Q^2 of 0.7352 and 0.6266 for test set respectively, and the designed 29 novel derivatives performed no less than the highest active compound with good ADME/T pharmacokinetic properties and medicinal chemistry friendliness.
CONCLUSIONS: Bulky groups in R_1, bulky groups with weak hydrophobicity in R_3, and potent hydrophobic substituted group with electronegative in R_2 from contour maps provided important insights for assessing and designing 29 novel NDRIs, which were considered as candidates for cognitive dysfunction with depression or other related neurodegenerative disorders.

Keywords: Cognitive dysfunctions, field-based QSAR, drug design, pharmacokinetic properties

1. Introduction

Depression is a common psychiatric disorder, affecting more than 350 million people around the world [1–4]. Cognitive dysfunctions as a core complication of depression, leads to serious problems in executive functioning, attention, learning processing speed and memory [5–7]. These functional impairments often are remitted as the mood symptoms improved, but still residual after remission of mood symptoms, which reduce the work abilities of patients [5,8,9]. These resulted in the crippling economic burden including not only direct costs for treatment, but also sizeable indirect costs for the absenteeism and poor productivity in the work [5,10]. As the World Health Organization predicts, depression will be

the leading cause of disease burden worldwide by 2030 [1,5]. Thus, recovering cognitive dysfunctions has been identified as the novel therapeutic strategy for depression [5,11,12].

As reported, prefrontal cortex (PFC), hippocampus, nucleus accumbens (NAc), amygdala, and ventral striatum were the common neuropathological platform for depression and cognitive dysfunction due to depression [4,13–15]. Neuropsychological and imaging evidence indicated the PFC plays a critical role in the control of cognitive function [14,16–18]. In the course of treatment, some improving cognitive function drugs preferentially targeted to PFC catecholamines, and the striatum and NAc might contribute to their therapeutic efficacy [14]. In these brain areas, the dysfunctional catecholaminergic signaling is the posited etiology of depression and related cognitive dysfunction especially for the catecholamine neurotransmitters norepinephrine (NE) and dopamine (DA), which are required for proper prefrontal functions acting as coordination with each other [15,19,20]. Moreover, the transporters of norepinephrine (hNET) and dopamine (hDAT) are distributed in PFC, striatum and nucleus accumbens, and hDAT is sparse and hNET is high density in the PFC while are opposite in striatum and nucleus accumbens [14,16]. Meanwhile, the hNET displays a high affinity for DA and plays a prominent role in DA clearance [16]. Thus selective NE reuptake inhibitors (sNRIs) merely could elevate both NE and DA in the PFC but with minimal effects on striatal and NAc DA [14], and selective DA reuptake inhibitors (sDRIs) mainly effected on striatal and NAc DA. In contrast, dual NE and DA reuptake inhibitors (NDRIs) performed more efficacy because they could impact on NE and DA level not only in PFC but also in striatal and NAc [20], and which of them with hNET > hDAT potency order could performed more effective in treatment of PFC-dependent diseases due to limit expression of hDAT in PFC and the relatively high affinity of DA for hNET compared to hDAT [15].

Recently, there are 4 NDRIs (Dexmethylphenidate, Dextroamphetamine, Dextromethamphetamine, Bupropion) used to improve cognitive dysfunction. The first three of them are reported to remit the cognitive dysfunction reduced by Attention-Deficit Hyperactivity Disorder (ADHD), but the risk of abuse potential and addictive for them limit their widespread use [15,21,22]. The last one bupropion, an aminoketone derivative is phase 4 clinical study in improving cognitive function for depression patients [5, 23]. However, its therapeutic effect is unsatisfactory attributed to the poorer clinical response [24]. Besides bupropion, none aminoketone derivatives of NDRIs antidepressants are currently in clinical trial, and only few are in pre-clinical.

In order to satisfy the strong need for antidepressants with improved cognitive dysfunction and enhanced efficacy, this work explored the Quantitative Structure-Activity Relationship (QSAR) characteristics of aminoketone derivatives based on the potent poses by molecular docking, which could be utilized as structural guidance for assessing and rationally designing more efficacious NDRIs candidates with hNET > hDAT potency order of cognitive dysfunction with depression or other related neurodegenerative disorders.

2. Materials and methods

2.1. Datasets preparation

This work collected 60 and 63 aminoketone derivatives with active data of hNET and hDAT from CHEMBL database [25] for field-based QSAR study as shown in Table 1. The datasets were randomly assigned 70% into training set of 42 molecules for hNET and 44 molecules for hDAT to generate QSAR models, and the rest of them as test sets were used to validate. The process of dividing datasets for both models should be considered the uniform distribution of compounds with as enough structural diversity

Table 1
The Glide gscore, experimental and predicted activities in data sets for selected QSAR models of hNET and hDAT

No.	R_1	R_2	R_3	Glide gscore		Experimental activity (PIC$_{50}$)		Predicted activity (PIC$_{50}$)		Prediction error [a]	
				hNET	hDAT	hNET	hDAT	hNET	hDAT	hNET	hDAT
1	CH$_3$	3-Cl	HN–(tBu)	-7.14	-7.37	5.73	6.18	5.55	5.89	-0.18	-0.29
2	C$_3$H$_7$	4-(O–C(=O)–)	N-pyrrolidine	-8.64	-6.21	7.64	6.81	7.39	6.68	-0.13	-0.19
3	C$_3$H$_7$	furan-4	N	-7.89	-5.29	7.03	6.91	6.81	6.70	-0.22	-0.21
4	C$_2$H$_5$	3,4-Cl	N	-7.21	-6.53	7.73	7.26	7.63	7.27	-0.10	0.01
5	(allyl)	3,4-Cl	N	-6.23	-6.53	7.60	7.74	7.44	7.79	-0.16	0.05
6★	(isobutenyl)	4-CH$_3$	N	-8.21	-5.78	7.75	8.23	7.23	7.84	-0.52	-0.39
7	(allyl)	4-CH$_3$	N	-6.34	-6.10	7.06	7.26	7.11	7.45	0.06	0.19
8♦	C$_3$H$_7$	4-Br	N	-6.98	-5.67	7.08	7.4	7.35	7.58	0.27	0.18
9	C$_3$H$_7$	4-I	N	-6.82	-5.83	7.33	7.50	7.75	7.77	0.42	0.27
10	C$_3$H$_7$	3,4-OH	N	-8.65	-6.00	8.12	7.38	7.60	7.36	-0.52	-0.02
11	C$_3$H$_7$	2-CH$_3$	N	-6.93	-6.84	7.71	7.20	7.15	6.64	-0.56	-0.56
12★	C$_3$H$_7$	3,4-Cl	N	-6.79	-5.83	7.68	7.37	7.83	8.02	0.15	0.65
13	C$_3$H$_7$	4-CH$_2$OH	N	-7.31	-5.90	7.91	7.35	7.58	6.65	-0.33	-0.70
14	C$_3$H$_7$	4-OH	N	-5.83	-7.20	7.06	7.30	7.30	6.68	0.24	-0.62
15	C$_3$H$_7$	4-F	N	-7.15	-6.37	6.77	6.73	7.44	7.27	0.67	0.54
16	C$_3$H$_7$	3-CH$_3$	N	-6.75	-7.05	8.03	7.20	7.01	7.32	-1.02	0.12
17♦	C$_3$H$_7$	(alkynyl)-4	N	-7.40	-6.31	7.71	7.93	7.60	7.74	-0.11	-0.19

Table 1, continued

No.	R	Substituent	Amine								
18*♦	C_3H_7	(phenyl ring)	N-pyrrolidine	-9.28	-5.82	7.93	7.40	7.34	6.78	-0.59	-0.62
19♦	C_3H_7	3,4~Cl	~NHC_4H_9	-5.73	-7.30	5.60	5.92	5.45	6.58	-0.15	0.66
20*♦	C_3H_7	4~H	N-pyrrolidine	-6.68	-6.44	7.25	7.28	7.44	7.35	0.19	0.07
21	C_3H_7	4~CH_3	N-pyrrolidine	-8.54	-5.95	7.95	7.79	7.61	7.17	-0.34	-0.62
22	C_3H_7	NO_2~4	N-pyrrolidine	-7.36	-6.45	6.28	5.96	6.95	6.27	0.67	0.31
23*	C_3H_7	$CH_3C(O)HN$~4	N-pyrrolidine	-8.23	-7.78	6.5	7.17	7.26	6.95	0.76	-0.22
24♦	C_3H_7	4~OCH_3	N-pyrrolidine	-8.25	-5.82	6.63	6.55	7.23	7.29	0.60	0.74
25*♦	C_3H_7	3~I	N-pyrrolidine	-6.16	-6.61	7.09	7.28	7.44	7.51	0.35	0.23
26	C_5H_{11}	3~Cl	HN-$C(CH_3)_3$	-7.33	-6.23	5.70	5.80	6.09	6.02	0.39	0.22
27♦	CH_3	3~Br	HN-$C(CH_3)_3$	-7.67	-7.84	5.25	6.29	5.25	5.89	0.00	-0.40
28	CH_3	3~Cl	HN-$C(CH_3)_3$	——	-7.26	——	5.70	——	5.97	——	0.27
29	C_6H_{13}	3~Cl	HN-$C(CH_3)_3$	-7.34	-5.41	5.31	6.87	5.62	6.86	0.31	-0.01
30	(isopropyl)	3~Cl	HN-$C(CH_3)_3$	-8.99	-6.88	6.44	6.36	6.31	6.75	-0.13	0.39
31♦	CH_3	3~Cl, 4~CH_3	HN-$C(CH_3)_3$	-8.11	-7.25	6.05	6.39	5.39	6.14	-0.66	-0.25
32	CH_3	3~CH_3, 4~Br	HN-$C(CH_3)_3$	-6.89	-7.51	5.79	6.02	5.57	6.09	-0.22	0.07
33	CH_3	4~Cl	HN-$C(CH_3)_3$	-8.26	-7.87	5.68	5.96	5.55	6.07	-0.13	0.11
34	CH_3	4~Br	HN-$C(CH_3)_3$	-7.99	-7.86	5.59	6.16	5.60	6.12	0.01	-0.04
35	C_3H_7	3,4~Cl	HN-$C(CH_3)_3$	-7.82	-5.59	7.37	7.51	7.06	7.26	-0.31	-0.25
36*	CH_3	4~CH_3	HN-$C(CH_3)_3$	-7.55	-7.43	5.63	5.71	5.31	5.91	-0.32	0.20
37	C_2H_5	3,4~Cl	HN-$C(CH_3)_3$	-8.09	-7.48	6.87	6.93	6.92	6.65	0.05	-0.28

Table 1, continued

38	⌇CH$_3$	3⌇Cl	⌇HN⟨	-8.38	-7.65	5.90	5.81	6.16	5.94	0.26	0.13
39♦	⌇CH$_3$	3⌇CH$_3$	⌇HN⟨	-6.38	-7.09	5.21	5.83	5.16	5.65	-0.05	-0.18
40	⌇C$_2$H$_5$	3⌇Cl	⌇HN⟨	-6.85	——	6.22	——	6.55	——	0.33	——
41★♦	⌇CH$_3$	3,4⌇Cl	⌇HN⟨	-7.12	-7.58	5.78	6.57	5.63	6.29	-0.15	-0.28
42	⌇C$_3$H$_7$	3⌇Cl	⌇HN⟨	-8.60	——	6.43	——	6.29	——	-0.14	——
43★♦	⌇CH$_3$	⌇H	⌇HN⟨	-6.51	-7.39	5.06	5.64	5.18	5.67	0.12	0.03
44	⌇CH$_3$	3⌇Cl	⌇N(H)▷	-7.78	-8.23	5.67	6.58	5.74	6.24	0.07	-0.34
45★	⌇CH$_3$	3⌇F	⌇HN⟨	-7.32	-7.31	5.19	5.84	5.23	5.71	0.04	-0.13
46	⌇C$_4$H$_9$	3⌇Cl	⌇HN⟨	-7.88	-5.84	6.40	7.16	6.68	6.94	0.28	-0.22
47	⌇CH$_3$	3,5⌇F	⌇HN⟨	——	-7.60	——	5.25	——	5.71	——	0.46
48★♦	⌇CH$_3$	3,4⌇F	⌇HN⟨	-7.29	-8.41	5.19	5.10	5.37	5.84	0.18	0.74
49	⌇CH$_3$	3,5⌇Cl	⌇HN⟨	-7.29	——	4.85	——	5.35	——	0.50	——
50★♦	⌇CH$_3$	3⌇Cl	⌇HN⟨	-6.51	-7.67	5.80	5.69	5.88	6.03	0.08	0.34
51	⌇CH$_3$	3⌇Cl	⌇N(piperidine)	-7.61	-7.72	5.34	5.76	6.20	5.97	0.86	0.21
52	⌇CH$_3$	3⌇OCH$_3$	⌇N(piperidine)	-7.66	-6.90	6.14	6.34	6.18	5.95	0.04	-0.39
53	⌇CH$_3$	3⌇OCH$_3$	⌇N(H)(cyclopentyl)	-6.47	-7.58	5.09	5.64	5.00	5.78	-0.09	0.14
54★	⌇CH$_3$	3⌇CH$_3$	⌇N(piperidine)	-7.54	-6.88	6.24	6.38	6.40	6.15	0.16	-0.23

Table 1, continued

No.	R1	R2	Amine								
55	CH₃	3-CH₃	cyclopentyl–NH	-6.40	-7.22	5.06	6.08	5.22	5.98	0.16	-0.10
56★◆	CH₃	3-F	piperidine	-7.65	-6.72	6.87	6.81	6.48	6.20	-0.39	-0.61
57★	CH₃	3-Br	piperidine	-7.48	-6.86	5.93	6.12	6.50	6.39	0.57	0.27
58★	CH₃	NO_2-3	piperidine	-7.94	-7.02	5.39	5.00	6.31	5.64	0.92	0.64
59◆	CH₃	3-Br	cyclopentyl–NH	-8.94	-7.67	5.60	6.07	5.32	6.21	-0.28	0.14
60◆	CH₃	3-F	cyclopentyl–NH	-9.12	-7.76	5.54	6.16	5.30	6.03	-0.24	-0.13
61★◆	(allene)	4-CH₃	pyrrolidine	-5.40	-6.81	6.46	6.64	6.95	7.45	0.49	0.81
62	CH₃	3-OCH₃	HN–tert-butyl	——	-7.07	——	5.44	——	5.22	——	-0.22
63	C₃H₇	N≡–4	pyrrolidine	——	-6.33	——	6.00	——	6.54	——	0.54
64	CH₃	3-Cl	cyclobutyl–NH	——	-7.09	——	6.59	——	6.15	——	-0.44
65★	CH₃	3-Cl	piperidine	-7.64	-6.88	5.60	6.07	6.51	6.39	0.91	0.32
66◆	CH₃	3-Cl	cyclopentyl–NH	——	-7.87	——	6.01	——	6.21	——	0.20
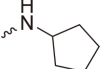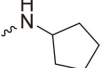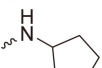
★Test set for hNET field based QSAR studies. ◆Test set for hDAT field based QSAR studies. [a]Prediction error = Predicted activity − Experimental activity.

and wide range activities as possible. The training and test sets of both models are demonstrated in Table 1.

2.2. Homology modeling and molecular docking

The potent poses of compounds for each target were identified based on the complexes of target-ligand achieved by molecular docking and prime minimization. Since there is no crystal structural data reported in Research Collaboratory for Structural Bioinformatics Protein Data Bank (RCSB PDB) [26], the 3D structures of hNET and hDAT need to be constructed by homology modeling performed in *SWISS-MODEL workspace* [27]. The template used to construct models was confirmed according to sequence

identity with targets by sequence alignment using ClustalW2 [23,28,29], and the stereochemical quality of built structures were checked by Ramachandran plot referenced our previous work [30–32].

The process of molecular docking was carried out in *Maestro* [33]. The first detailed work, active compounds of hNET and hDAT were collected from CHEMBL, and then their structures were preprocessed by the *LigPrep* [34] using *OPLS-2005 force field* [35]. The ionized state was assigned by *Epik* [36] at pH value of 7.0 ± 2.0. Secondly, to prepare hNET and hDAT structures for docking, the *Protein Preparation Wizard* module in *Maestro* [33] was used to add hydrogen atoms, assign partial charges using OPLS-2005 force field, assign protonation states and minimize the structure. The minimization was terminated when the root mean square deviation reached the maximum value of 0.30 Å. Finally, docking grid boxes were defined using the *Receptor Grid Generation* tool in *Glide* [37] by centroid of corresponding ligands from the template structures, and the prepared structures were docked in binding site of each target via standard precision (SP) in Schrödinger *Glide* module [37]. The preferred ligand was further rescored to calculate relative binding free energies using *prime* [38] MM-GBSA method at default.

2.3. Field-based QSAR models construction and validation

Field-based QSAR studies were performed on *Field-based QSAR* module [39] in *Maestro* [33]. The potent poses were superimposed to bupropion by SMARTS method based on common scaffold in *Flexible ligand alignment* module. The field-based QSAR models were constructed by training sets at the extended Gaussian field, and the maximum PLS factors was set 5 for hNET and hDAT. The best models for each target were identified by statistical robustness, and their stabilities and predictive abilities were validated by the testing sets with leave-one-out (LOO) cross-validation methods. The most important statistics are the test set statistics including RMSE, Q^2, and Pearson-r, which indicate how good the predictions are. If the predictions are not improving (much) as the number of PLS factors increases, the extra factors are not adding to the model and the model is probably over-fit. Scatter plots illustrated the correlation between the observed and predicted activity of all compounds for selected models. Moreover, the 3D contour maps for Gaussian steric, electrostatic, hydrophobic, hydrogen bond donor/acceptor, and aromatic ring fields were analyzed in QSAR Visualization module.

2.4. ADME/T and chemical synthetize properties predicted for candidates

In order to obtain effective drugs, this work evaluated the ADME/T properties of the designed NDRIs by the pkCSM (http://biosig.unimelb.edu.au/pkcsm/prediction) and ADMETlab online server (http://admet.scbdd.com/calcpre/index/). On the SwissADME online server (http://www.swissadme.ch/index.php), the problematic fragments in novel candidates were identified by the complementary pattern recognition method of PAINS (pan assay interference compounds) and Brenk filter. Moreover, the synthetic accessibilities (SA) were evaluated to demonstrate the synthetic complexities for molecules. A molecule with SA score closer to 10 was considered difficult to synthetic, while was considered as easy with closer to 1.

3. Results and discussion

3.1. Homology modeling and validation for hNET and hDAT

The X-ray crystal structures of *Drosophila melanogaster* dopamine transporter (dDAT, PDB ID: 4XPH) showed high sequence identity with hNET (60.98%) and hDAT (55.83%), and showed higher sequence
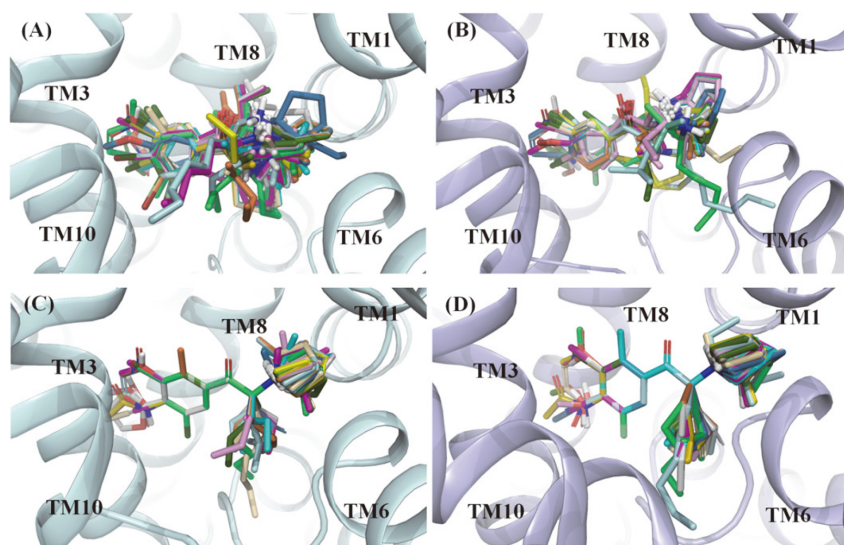
Fig. 1. Docking poses (A and B) and superimposed poses (C and D) template as bupropion of NDRIs compounds in the binding pocket of hNET and hDAT. The hNET (palecyan) and hDAT (lightblue) were shown in ribbon representation.

identity in binding site as the same as our previous work (69.05% and 78.57% for hNET and hDAT, respectively) [31]. Homology models of hNET and hDAT were constructed by dDAT as template, and the stereochemical quality and accuracy of models were illustrated by Ramachandran plot. Residues of models in allowed regions were 99.8% and 100% for hNET and hDAT respectively, indicating the reasonability of obtained models.

3.2. The selected the potent poses by molecular docking and MM-GBSA prime

In this work, re-docking of 4XPH was first performed to validate the credibility of docking protocol. The binding pose of DCP in dDAT achieved by molecular docking was close to the original conformation with 0.474 of root mean square deviation (RMSD), indicating the validity of the docking protocol. Then, all active molecules were docked in each target using the same parameter settings as re-docking, and the obtained all complexes were minimized by MM-GBSA prime. Finally, the potent pose of bupropion was identified as the same as our previous work [31], including the electrostatic interaction between ammonium moiety and Asp75/Asp79 in hNET/hDAT recognition, and hydrophobic interactions formed in corresponding sub-sites for the other two groups. For other molecules, the docking poses were selected based on the docking score and the orientation of bupropion. Figure 1A and B show all selected poses gathered in the binding site surrounded by TM1, 3, 6, 8 and 10.

3.3. Constructing and assessing of filed-based QSAR models for hNET and hDAT

All selected poses for hNET and hDAT were superimposed template as bupropion as demonstrated in Fig. 1C and D. In this work, 10 filed-based QSAR models were constructed using superimposed training sets compounds for hNET and hDAT, and the reliabilities of models were assessed by testing sets. All QSAR statistics are collected in Table 2.

For QSAR models of hNET, the values of R^2 for the partial least square regression rose as increased factors, while the last 2 models should be discarded due to the lower stability value than the R^2, which

Table 2
PLS statistics of hNET and hDAT field-based QSAR models

Factors	SD	R^2	R^2_{CV}	R^2 scramble	Stability	F	P	RMSE	Q^2	Pearson-r
hNET QSAR models										
1	0.6121	0.6143	0.5168	0.1873	0.987	63.7	8.38e-010	0.51	0.6882	0.8458
2	0.4662	0.7818	0.5428	0.3378	0.906	69.9	1.28e-013	0.50	0.6985	0.8836
3[a]	0.3944	0.8479	0.5873	0.4553	0.880	70.6	1.35e-015	0.47	0.7352	0.8776
4	0.3251	0.8993	0.6186	0.5658	0.842	82.7	6.29e-018	0.46	0.7469	0.8830
5	0.2841	0.9252	0.6150	0.6456	0.808	89.1	3.04e-019	0.39	0.8199	0.9145
hDAT QSAR models										
1	0.5559	0.4800	0.3669	0.2074	0.984	38.8	1.88e-007	0.43	0.6582	0.8134
2	0.4580	0.6554	0.4602	0.3296	0.956	39.0	3.27e-010	0.46	0.6015	0.7784
3[b]	0.3497	0.8040	0.5107	0.4613	0.880	54.7	3.24e-014	0.45	0.6266	0.8072
4	0.2751	0.8817	0.5727	0.5402	0.826	72.7	1.52e-017	0.49	0.5471	0.7644
5	0.2407	0.9118	0.5981	0.6056	0.798	78.6	5.55e-019	0.53	0.4804	0.7239

[a]selected Field-based QSAR model for hNET. [b] selected Field-based QSAR model for hDAT.
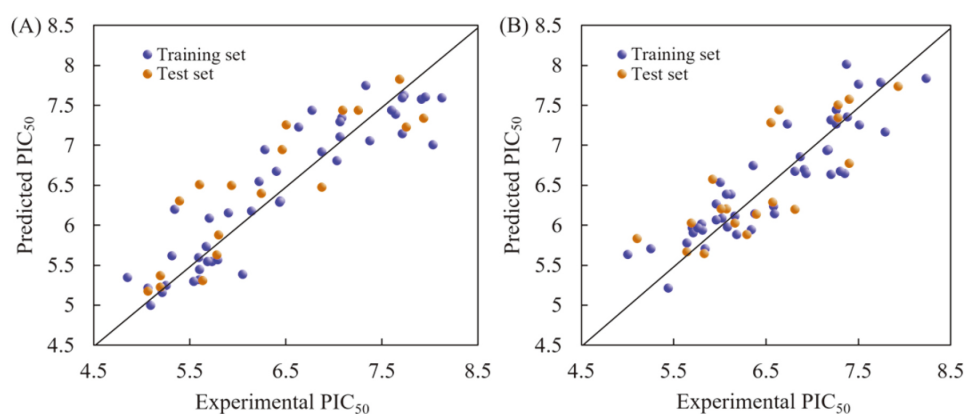

Fig. 2. Correlation plots of the predicted and experimental PIC_{50} values for training and test sets of hNET (A) and hDAT (B).

indicating the over-fitting of them. The best model of 3 factor performed good predictive and descriptive power based on QSAR statistics with 0.8479 for R^2 and 0.5873 for R^2_{cv}. Moreover, the $1.35e^{-15}$ for P value further indicated great degree of confidence. The reliability of model 3 was assessed by independent testing set of 18 compounds, and the value of Q^2 for the predicted activities was 0.7352 suggesting its potent capability in predicting extend molecules. Besides, 0.8776 for Pearson-r showed a good correlation between predicted and observed activity for the test set, which further confirmed models' reliability (robustness). As the similar analysis of QSAR statistics among hDAT models, the model of 3 factor was the best selection owing to the high linear correlation for training set ($R^2 = 0.8040$) and the potent capability in predicting testing set ($Q^2 = 0.6266$) without over-fitting. The experimental and predicted activities in data sets for selected models collected in Table 1 and evenly distributed around the diagonal as illustrated in Fig. 2, which intuitively verified the effectiveness of models.

3.4. Contour maps analyses of QSAR models for hNET and hDAT

3D contour maps of 6 extended Gaussian fields referenced bupropion (compound 1) are illustrated in Fig. 3, which provide information about the contribution of substituents on phenyl-aminoketone scaffold to the activity for each target. As shown in Fig. 3, steric and hydrophobic fields performed more potent
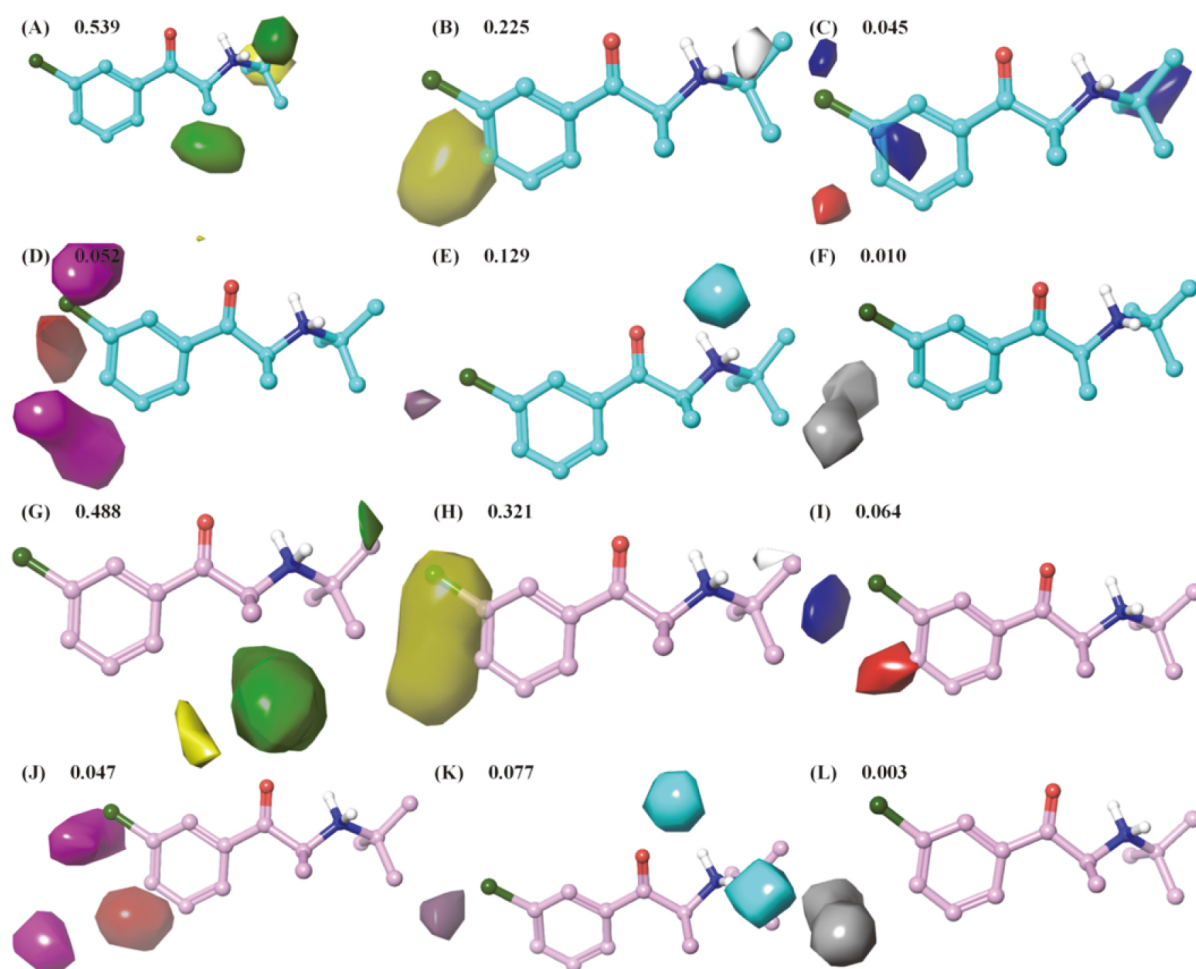
Fig. 3. 3D contour maps of 6 extended Gaussian fields referenced bupropion for hNET and hDAT field-based QSAR models. A-F and G-L were steric, hydrophobic, electrostatic, hydrogen bond acceptor, hydrogen bond donor and aromatic ring field contour maps based on bupropion in hNET (cyan) and hDAT (pink) models, respectively. The colors of favorable and unfavorable regions were green and yellow for steric fields, yellow and white for hydrophobic field, blue and red for electrostatic fields, red and magenta for hydrogen bond acceptor, purple and cyan for hydrogen bond donor and orange and gray for aromatic ring field, respectively.

contribution to activity than other 4 fields with 0.539 and 0.225 respectively for hNET, and with 0.484 and 0.323 respectively for hDAT. Thus, the volume and hydrophobicity of substituents on phenyl-aminoketone played major roles in regulating activity.

From the steric contour maps (Fig. 3A), there were 2 green and 1 yellow contour regions around aminoketone moiety, with green meaning bulky groups are favored and yellow meaning bulky groups are disfavored. The green contour maps at R_1 (substituted-carbonyl) were incarnated by the increased activities of compounds 1 (5.73), 40 (6.22) and 42 (6.43) with methyl, ethyl and propyl group respectively. However, compounds 46 (6.40), 26 (5.70) and 29 (5.31) with butyl, amyl and hexyl are gradually weaker than 42 for hNET, which demonstrated the larger stereoscopic space is not meaning blindly the longer carbon chain. This opinion was effectively proved by compounds 30 (6.44) and 46 (6.40) with the same carbon atoms for isobutyl and butyl group, the same condition was found in compounds 7 (7.06) and

21 (7.95) with propenyl and propyl. Moreover, the green and yellow contour maps at R_3 (substituted-ammonium) signified the large group with short carbon chain was beneficial to increase the activity. It was reflected by the weak activity of compound 19 (5.60) with butyl rather than bulky tertiary butyl in compound 1, and by compound 53 (5.09) with cyclopentyl-ammonium comparing with the larger piperidyl group in 52 (6.14). The similarities of steric contour maps between hDAT (Fig. 3G) and hNET at R_1 and R_3 meant that the large moieties in these regions are favor of increasing activities for hDAT.

The yellow contour map of hydrophobicity was mainly sited at R_2 (substituted aromatics) as illustrated in Fig. 3B and H, which demonstrated introducing the higher hydrophobic group would increase the activities against targets. The result was confirmed by 1 (7.91 for hNET, 7.35 for hDAT) with 4-methanol group versus 14 (7.06, 7.30) replaced by 4-phenolic hydroxyl, 9 (7.33, 7.50) comparing with 15 (6.77, 6.73) and 21 (7.95, 7.79) in contrast to 2 (7.64, 6.81). Moreover, the larger yellow polyhedron covering meta-position of R_2 for hDAT (Fig. 3H) comparing with hNET (Fig. 3B), which supplied guidance to regulate the balance of activity for two targets. Conversely, the white contour at R_3 (Fig. 3B and H) indicated that introducing weaker hydrophobic group would improve the inhibition of targets. For example, the replacement of cyclopentyl in this region by piperidyl with lower hydrophobicity could increase the activity. This regulation could be seen from compound 52 (6.14, 6.34) versus 53 (5.09, 5.64), 54 (6.24, 6.38) in contrast to 55 (5.06, 6.08), respectively.

The electrostatic field contour maps are illustrated in Fig. 3C and I. The regions in red surrounded at para-position of R_2 implied where negative charge groups enhanced bioactivity, whereas the regions in blue sited at meta-position of R_2 purported positive charge groups improved the activity. The orderliness for para-position of R_2 could be adequately reflected by the decrease activities of compounds 21 (7.95, 7.79), 2 (7.64, 6.81) and 22 (6.26, 5.96), which is due to the gradual reduction of electronegativities for methyl, methyl formate and nitro, respectively. Meanwhile, it also appeared in compounds 9 (7.33, 7.50), 8 (7.08, 7.4), 15 (6.77, 6.73) with increasing of electronic deficiency for iodine, bromine and fluorine atom. At meta-position of R_2, because of the more electropositive of carbon atom in naphthalene at blue region, compound 18 (7.93, 7.40) performed higher activity contrasting to compound 2 (7.64, 6.81) with methyl or 23 (6.5, 7.17) with oxygen atom in carbonyl. Additionally, the oxygen atom with negative charge in meta-nitro of compound 58 intersected the blue area, therefore, it performed the weakest active among similar compounds 54, 56, 57, 59, 60.

The H-bond acceptor contour maps (Fig. 3D and J) closed to R_2, which indicated that introduction of H-bond acceptor atom in red region is favorable while magenta areas stood for the opposite. This might be one reason for compound 13 with hydroxy as H-bond acceptor atom performed potent activity for hNET and hDAT. The purple contours in Fig. 3E and K signify H-bond donor was beneficial, while cyan contours were unfavored to increase activity. This might could be explained by the hydrogen bond between protonated nitrogen (NH^+) in R_3 and negative charged oxygen (O^-) of Asp75/Asp79 were essential for drugs recognition of hNET and hDAT in previous work [31,40]. Finally, from gaussian aromatic ring contours as displayed in Fig. 3F and L, the gray polyhedron surrounding the para-position of R_2 suggesting that it was not prominently effectual to increase the activity by introducing the aromatic group.

Considering all discussed above, this work supplied the graphical description of the structural features for designing novel NDRIs. In order to improve the activity, researchers could replace the methyl by the bulky groups with suitable carbon chain at R_1, and/or with additional weak hydrophobicity at R_3. Moreover, hydrophobic and electronegative substituted at R_2 should be helpful for enhancing the effectiveness. Meanwhile, designer could regulate the active balance between hNET and hDAT by changing the hydrophobicity with obvious contribution to activity of meta-position of R_2. At last but the most important, it was necessary to retain the protonizable nitrogen in ammonium group to form hydrogen bond for recognizing by targets.

Table 3
The predicted activities of designed novel derivatives by selected hNET and hDAT QSAR models

No.	R_1	R_2	R_3	Predicted activity (PIC_{50})		No.	R_1	R_2	R_3	Predicted activity (PIC_{50})	
				hNET	hDAT					hNET	hDAT
D1§		4~CF_3		8.23	7.64	D16§		3,4~CF_3		8.59	7.97
D2‡		4~CF_3		8 01	7.41	D17§		3~CH_3, 4~CF_3		8.41	7.71
D3‡		4~CF_3		8.11	7.28	D18‡		3~CH_3, 4~CF_3		8.12	7.54
D4‡		3~CH_3, 4~CF_3		8.08	7.24	D19§		3,4~CF_3		8.25	7.79
D5§		3,4~CF_3		8.21	7.49	D20§		3~OCH_3, 4~CF_3		8.30	7.12
D6§		3,4~CF_3		8.34	7.85	D21§		3~OCF_3, 4~CF_3		8.69	8.16
D7§		3~CH_3, 4~CF_3		8.20	7.60	D22§		3~OH 4~CF_3		8.39	7.69
D8‡		3,4~CF_3		8.11	7.62	D23§		3~$C(O)OCH_3$, 4~CF_3		8.39	7.27
D9‡		4~CH_3		8.13	7.48	D24§		3~OCH_3, 4~HSO_3		8.28	7.03
D10§		4~CF_3		8.44	7.74	D25§		3~OCF_3, 4~HSO_3		8.18	7.87
D11‡		4~CF_3		8.15	7.57	D26‡		3~OH, 4~HSO_3		8.04	7.41
D12‡		4~CF_3		8.19	7.39	D27§		3~OCF_3, 4~Cl		8.48	8.04
D13‡		3~CH_3, 4~CF_3		8.16	7.36	D28§		3~OCH_3, 4~Cl		8.27	7.29
D14§		3,4~CF_3		8.30	7.60	D29§		3~OCF_3, 4~OCH_3		8.28	7.61
D15§		3~CF_3, 4~CH_3		8.23	7.71						

‡Molecules with active as the high active NDRI compound 10. §Molecules with more active than compound 10.

Table 4
ADME/T and medicinal chemistry friendliness properties of 29 designed molecules with high activities

No	Absorption	Distribution			Metabolism								Excretion	Toxicity			Medicinal chemistry		
					Substrate			Inhibitor											
	HIA[a]	VDss[b]	BBB[c]	CNS[d]	2D6	3A4	1A2	1A2	2C19	2C9	2D6	3A4	CLtot[e]	AMES	Hepato toxicity	Skin sensitization	PAIN[f]	Brenk[g]	SA[h]
D1	92.35	1.10	0.55	−1.76	Yes	Yes	Yes	No	No	Yes	No	No	1.03	No	Yes	No	0	0	2.85
D2	95.22	1.00	0.60	−1.59	No	Yes	Yes	No	No	Yes	No	No	1.09	No	No	No	0	0	2.74
D3	93.02	1.08	0.71	−1.31	Yes	Yes	Yes	Yes	No	Yes	No	No	1.00	No	Yes	No	0	0	2.61
D4	93.46	1.13	0.72	−1.35	Yes	Yes	Yes	Yes	No	Yes	No	No	0.97	No	Yes	No	0	0	2.76
D5	90.67	0.95	0.66	−1.33	Yes	Yes	No	No	No	Yes	No	No	0.71	No	Yes	No	0	0	2.91
D6	90.08	0.86	0.51	−1.96	No	Yes	No	No	No	No	No	No	0.73	No	Yes	No	0	0	3.15
D7	92.87	1.09	0.56	−1.81	Yes	Yes	Yes	No	No	Yes	No	No	0.99	No	Yes	No	0	0	3.00
D8	92.71	0.82	0.59	−1.79	No	Yes	No	No	No	Yes	No	Yes	0.78	No	Yes	No	0	0	3.04
D9	94.34	1.34	0.57	−1.66	Yes	Yes	Yes	No	No	Yes	No	No	1.14	No	Yes	Yes	0	0	2.78
D10	91.96	1.12	0.54	−1.80	No	Yes	Yes	No	No	Yes	No	No	0.97	No	Yes	No	0	0	2.96
D11	94.83	1.02	0.59	−1.64	Yes	Yes	Yes	No	No	Yes	No	No	1.05	No	No	No	0	0	2.85
D12	92.63	1.12	0.69	−1.29	Yes	Yes	Yes	Yes	No	Yes	No	No	0.95	No	Yes	No	0	0	2.71
D13	93.07	1.16	0.70	−1.34	Yes	Yes	Yes	Yes	No	Yes	No	No	0.92	No	Yes	No	0	0	2.86
D14	90.28	0.98	0.65	−1.31	Yes	Yes	Yes	No	No	Yes	No	No	0.66	No	Yes	No	0	0	3.01
D15	92.88	0.81	0.69	−1.85	Yes	No	Yes	No	No	Yes	No	No	0.92	No	Yes	No	0	0	3.17
D16	89.69	0.88	0.49	−2.00	No	Yes	No	No	No	No	No	No	0.68	No	No	No	0	0	3.26
D17	92.49	1.11	0.55	−1.86	Yes	Yes	Yes	No	No	Yes	No	No	0.94	No	No	No	0	0	3.11
D18	95.12	1.04	0.60	−1.70	No	Yes	Yes	No	No	Yes	No	No	1.01	No	No	No	0	0	3.00
D19	92.32	0.85	0.57	−1.84	No	Yes	No	No	No	Yes	No	Yes	0.73	No	No	No	0	0	3.15
D20	95.57	0.81	0.61	−1.84	No	Yes	Yes	No	No	Yes	No	Yes	0.95	No	No	No	0	0	3.28
D21	89.06	0.59	0.48	−2.12	No	Yes	No	No	No	No	No	No	0.44	No	No	No	0	0	3.58
D22	91.38	0.96	0.16	−1.85	Yes	Yes	No	No	No	Yes	No	Yes	0.90	No	No	No	0	0	3.18
D23	92.32	0.74	−0.14	−2.10	No	No	Yes	No	No	No	No	No	0.91	No	No	No	0	0	3.58
D24	96.19	0.83	0.72	−1.86	No	No	Yes	Yes	No	Yes	No	No	1.13	No	No	No	0	0	3.16
D25	92.33	0.58	0.76	−2.01	No	No	Yes	No	No	No	No	No	0.69	No	No	No	0	0	3.38
D26	94.57	1.04	0.21	−1.24	No	No	No	No	No	No	No	No	1.16	No	No	No	0	0	2.97
D27	90.87	0.52	0.74	−2.01	No	No	Yes	No	No	No	No	No	0.69	No	No	No	0	0	3.33
D28	94.73	0.77	0.68	−1.86	No	Yes	No	No	No	Yes	No	No	1.12	No	No	No	0	0	3.17
D29	91.61	0.68	0.44	−2.09	No	Yes	Yes	No	No	No	No	No	0.76	No	No	No	0	0	3.54

aHIA: human intestine absorption, the value with less than 30% was considered poorly absorbed. bVDss: Volume of Distribution at steady state, the value was considered low if below 0.71 L/kg (lgoVDss < −0.15) and high if above 2.81 L/kg (lgoVDss > 0.45). cBBB: This work measured the logarithmic ratio of brain to plasma drug concentrations (logBBB) for candidates in vivo in animal models. A molecule with logBBB > 0.3 considered to readily cross the blood-brain barrier, while it was poorly distributed to the brain if logBBB < −1. dCNS: Central Nervous System, this work measured permeability-surface area product (logPS) for CNS, comounds with a logPS > −2 were considered to penetrate the CNS, while those with logPS < −3 were considered as unable to penetrate. eCLtot: Total Clearance (log(CLtot)). fPAINS: pan assay interference compounds. gBrenk: Brenk filter. hSA: synthetic accessibilities, SA score closer to 10 means difficult to synthetic, while closer to 1 means easy.

3.5. Design of novel derivatives

According to the information based on compound 1 provided by Field-based QSAR models, firstly this work replaced methyl of R_1 by cyclopentyl, cyclopentadienyl, cyclohexyl and phenyl, meanwhile introduced cyclopentyl, cyclohexyl, pyrrolyl, piperidyl at R_3. Secondly, the designed compounds were optimized by bring methyl, trifluoromethyl, methoxy, trifluoromethoxy and formate group in R_2, and regulated the active balance for hNET and hDAT by changing the hydrophobicity of substituent between meta- and para-position. Additionally, Other useful proposals could be performed to import the electronegative group in para-position of R_2 to yield goo candidates, such as methoxy, sulfo group and so on. Finally, 29 novel derivatives were designed and their activities were predicted by selected models of hNET and hDAT as collected in Table 3. All designed candidates performed with hNET > hDAT potency order, and their inhibitive ability were no less than the highest active NDRI compound 10.

3.6. ADME/T profiles and medicinal chemistry friendliness properties of candidates

The ADME/T properties and medicinal chemistry of 29 high active candidates were predicted using pre-ADMET web servers, and the results are shown in Table 4. As results, the rang of HIA was from 89.056% to 98.477%, indicating that all candidates performed high absorption properties from intestine. The VDss of most molecules was between 0.71 and 2.81 L/kg, which meant that they were evenly distributed in the plasma and in tissues, while compounds D21, D25, D27 and D29 with low 0.71 L/kg were distributed more in the plasma rather than in tissues. There was no compound to be considered as poorly distributed to the brain and unable to penetrate the CNS according BBB and CNS permeability. For metabolism, all designed molecules were predicted as substrates for the CYP450 2D6/3A4/1A2 subtype, which indicated they could be metabolized by P450 isoforms. In addition, compound D6, D16, D25, D26, D27 and D29 could not inhibit the CYP450 family, whereas the other compounds might inhibit the CYP450 1A2/2C19/2C9/2D6/3A4 subtype. The predicted total clearance of all compounds demonstrated they could be cleared by combing hepatic and renal tissue. Based on the predicted the toxicity, some candidates would be harmful for the liver, and only a few compounds were likely to be associated with skin sensitization, and none of them performed mutagenic potency. Finally, as shown the medicinal chemistry friendliness properties in Table 4, there was no problematic fragment in novel compounds assessing by PAINS and Brenk filter. The SA of all designed candidates ranged from 2.85 to 3.58, indicating the low synthetic complexity of structure and high synthetic feasibility. Taking all predicted ADMET properties and medicinal chemistry profiles into consideration, the designed 29 novel derivatives could be served as lead compounds for further development of NDRIs.

4. Conclusions

This work established firstly field-based QSAR models of aminoketone derivatives as hNET and hDAT reuptake inhibitors based on the potent poses by molecular docking, and the best models performed good predictability in in/external validations and reliability. According to the contour maps of QSAR models for hNET and hDAT, three strategies were proposed to improve the activity: (I) the bulky groups with suitable carbon chain at R_1 and R_3, (II) the additional weak hydrophobicity at R_3 with a precondition of protonizable nitrogen for recognizing by targets, and (III) the potent hydrophobic and electronegative substituted in R_2 with changing the hydrophobicity to regulate the active balance between hNET and hDAT at its meta site. These results provide new insights into the key structural factors affecting activity

to two targets, which could be further utilized as structural and energetic blueprints for assessing and discovering novel NDRIs with assigned potency order. Moreover, the designed 29 novel derivatives performed no less than the highest active NDRI compound 10, and all of them exhibited good ADME/T pharmacokinetic properties and medicinal chemistry friendliness, which could be considered as the NDRIs lead compounds for cognitive dysfunction with depression or other related neurodegenerative disorders.

Acknowledgments

Conflict of interest

The authors declare that they have no conflict of interest.

References

[1] Madhav KC, Sherchand SP, Sherchan S. Association between screen time and depression among US adults. Prev Med Rep. 2017; 8: 67. doi: 10.1016/j.pmedr.2017.08.005.

[2] Zhang Y, Zheng GX, Fu TT, Hong JJ, Li FC, Yao XJ, et al. The binding mode of vilazodone in the human serotonin transporter elucidated by ligand docking and molecular dynamics simulations. Phys Chem Chem Phys. 2020; 22(9): 5132. doi: 10.1039/c9cp05764a.

[3] Xue WW, Fu TT, Zheng GX, Tu G, Zhang Y, Yang FY, et al. Recent advances and challenges of the drugs acting on monoamine transporters. Curr Med Chem. 2020; 27(23): 3830. doi: 10.2174/0929867325666181009123218.

[4] Xue WW, Wang PP, Tu G, Yang FY, Zheng GX, Li XF, et al. Computational identification of the binding mechanism of a triple reuptake inhibitor amitifadine for the treatment of major depressive disorder. Phys Chem Chem Phys. 2018; 20(9): 6606. doi: 10.1039/c7cp07869b.

[5] Baune BT, Brignone M, Larsen KG. A Network Meta-Analysis comparing effects of various antidepressant classes on the Digit Symbol Substitution Test (DSST) as a measure of cognitive dysfunction in patients with major depressive disorder. Int J Neuropsychopharmacol. 2018; 21(2): 97. doi: 10.1093/ijnp/pyx070.

[6] Oliveira MR, Chenet AL, Duarte AR, Scaini G, Quevedo J. Molecular mechanisms underlying the anti-depressant effects of resveratrol: a review. Mol Neurobiol. 2018; 55(6): 4543. doi: 10.1007/s12035-017-0680-6.

[7] Fu TT, Zheng GX, Tu G, Yang FY, Chen YZ, Yao XJ, et al. Exploring the binding mechanism of metabotropic glutamate receptor 5 negative allosteric modulators in clinical trials by molecular dynamics simulations. Acs Chem Neurosci. 2018; 9(6): 4192. doi: 10.1021/acschemneuro.8b00059.

[8] Schaefer JD, Scult MA, Caspi A, Arseneault L, Belsky DW, Hariri AR, et al. Is low cognitive functioning a predictor or consequence of major depressive disorder? A test in two longitudinal birth cohorts. Dev Psychopathol. 2017; 1. doi: 10.1017/S095457941700164X.

[9] Targum SD, Wedel PC, Fava M. Changes in cognitive symptoms after a buspirone-melatonin combination treatment for Major Depressive Disorder. J Psychiatr Res. 2015; 68: 392. doi: 10.1016/j.jpsychires.2015.04.024.

[10] Ekman M, Granstrom O, Omerov S, Jacob J, Landen M. The societal cost of depression: evidence from 10,000 Swedish patients in psychiatric care. J Affect Disord. 2013; 150(3): 790. doi: 10.1016/j.jad.2013.03.003.

[11] Bortolato B, Miskowiak KW, Kohler CA, Maes M, Fernandes BS, Berk M, et al. Cognitive remission: a novel objective for the treatment of major depression? BMC Med. 2016; 14: 9. doi: 10.1186/s12916-016-0560-3.

[12] Salagre E, Sole B, Tomioka Y, Fernandes BS, Hidalgo-Mazzei D, Garriga M, et al. Treatment of neurocognitive symptoms in unipolar depression: a systematic review and future perspectives. J Affect Disord. 2017; 221: 205. doi: 10.1016/j.jad.2017.06.034.

[13] Levada OA, Troyan AS. Insulin-like growth factor-1: a possible marker for emotional and cognitive disturbances, and treatment effectiveness in major depressive disorder. Ann Gen Psychiatry. 2017; 16: 38. doi: 10.1186/s12991-017-0161-3.

[14] Schmeichel BE, Berridge CW. Neurocircuitry underlying the preferential sensitivity of prefrontal catecholamines to low-dose psychostimulants. Neuropsychopharmacology. 2013; 38(6): 1078. doi: 10.1038/npp.2013.6.

[15] Bymaster FP, Golembiowska K, Kowalska M, Choi YK, Tarazi FI. Pharmacological characterization of the norepinephrine and dopamine reuptake inhibitor EB-1020: implications for treatment of attention-deficit hyperactivity disorder. Synapse. 2012; 66(6): 522. doi: 10.1002/syn.21538.

[16] Spencer RC, Devilbiss DM, Berridge CW. The cognition-enhancing effects of psychostimulants involve direct action in the prefrontal cortex. Biol Psychiatry. 2015; 77(11): 940. doi: 10.1016/j.biopsych.2014.09.013.

[17] Miceli M, Gronier B. Psychostimulants and atomoxetine alter the electrophysiological activity of prefrontal cortex neurons, interaction with catecholamine and glutamate NMDA receptors. Psychopharmacology. 2015; 232(12): 2191. doi: 10.1007/s00213-014-3849-y.

[18] Xue WW, Wang PP, Li B, Li YH, Xu XF, Yang FY, et al. Identification of the inhibitory mechanism of FDA approved selective serotonin reuptake inhibitors: an insight from molecular dynamics simulation study. Phys Chem Chem Phys. 2016; 18(4): 3260. doi: 10.1039/c5cp05771j.

[19] Park JE, Song C, Choi K, Sim T, Moon B, Roh EJ. Synthesis and biological evaluation of novel 3,4-diaryl lactam derivatives as triple reuptake inhibitors. Bioorg Med Chem Lett. 2013; 23(20): 5515. doi: 10.1016/j.bmcl.2013.08.062.

[20] Xing B, Li YC, Gao WJ. Norepinephrine versus dopamine and their interaction in modulating synaptic function in the prefrontal cortex. Brain Res. 2016; 1641(Pt B): 217. doi: 10.1016/j.brainres.2016.01.005.

[21] Pliszka S, Issues AWGoQ. Practice parameter for the assessment and treatment of children and adolescents with attention-deficit/hyperactivity disorder. J Am Acad Child Adolesc Psychiatry. 2007; 46(7): 894. doi: 10.1097/chi.0b013e318054e724.

[22] Schmeichel BE, Zemlan FP, Berridge CW. A selective dopamine reuptake inhibitor improves prefrontal cortex-dependent cognitive function: potential relevance to attention deficit hyperactivity disorder. Neuropharmacology. 2013; 64: 321. doi: 10.1016/j.neuropharm.2012.07.005.

[23] Wang PP, Zhang XY, Fu TT, Li S, Li B, Xue WW, et al. Differentiating physicochemical properties between addictive and nonaddictive ADHD drugs revealed by molecular dynamics simulation studies. ACS Chem Neurosci. 2017; 8(6): 1416. doi: 10.1021/acschemneuro.7b00173.

[24] Bruder GE, Alvarenga JE, Alschuler D, Abraham K, Keilp JG, Hellerstein DJ, et al. Neurocognitive predictors of antidepressant clinical response. J Affect Disord. 2014; 166: 108. doi: 10.1016/j.jad.2014.04.057.

[25] Gaulton A, Hersey A, Nowotka M, Bento AP, Chambers J, Mendez D, et al. The ChEMBL database in 2017. Nucleic Acids Res. 2017; 45(D1): D945. doi: 10.1093/nar/gkw1074.

[26] Goodsell DS, Zardecki C, Di Costanzo L, Duarte JM, Hudson BP, Persikova I, et al. RCSB protein data bank: enabling biomedical research and drug discovery. Protein Sci. 2020; 29(1): 52. doi: 10.1002/pro.3730.

[27] Waterhouse A, Bertoni M, Bienert S, Studer G, Tauriello G, Gumienny R, et al. SWISS-MODEL: homology modelling of protein structures and complexes. Nucleic Acids Res. 2018; 46(W1): W296. doi: 10.1093/nar/gky427.

[28] Larkin MA, Blackshields G, Brown NP, Chenna R, McGettigan PA, McWilliam H, et al. Clustal W and Clustal X version 2.0. Bioinformatics. 2007; 23(21): 2947. doi: 10.1093/bioinformatics/btm404.

[29] Zheng GX, Xue WW, Yang FY, Zhang Y, Chen YZ, Yao XJ, et al. Revealing vilazodone's binding mechanism underlying its partial agonism to the 5-HT1A receptor in the treatment of major depressive disorder. Phys Chem Chem Phys. 2017; 19(42): 28885. doi: 10.1039/c7cp05688e.

[30] Wang PP, Yang FY, Yang H, Xu XF, Liu D, Xue WW, et al. Identification of dual active agents targeting 5-HT1A and SERT by combinatorial virtual screening methods. Biomed Mater Eng. 2015; 26(Suppl 1): S2233. doi: 10.3233/BME-151529.

[31] Wang PP, Fu TT, Zhang XY, Yang FY, Zheng GX, Xue WW, et al. Differentiating physicochemical properties between NDRIs and sNRIs clinically important for the treatment of ADHD. Biochim Biophys Acta Gen Subj. 2017; 1861(11 Pt A): 2766. doi: 10.1016/j.bbagen.2017.07.022.

[32] Zheng GX, Yang FY, Fu TT, Tu G, Chen YZ, Yao XJ, et al. Computational characterization of the selective inhibition of human norepinephrine and serotonin transporters by an escitalopram scaffold. Phys Chem Chem Phys. 2018; 20(46): 29513. doi: 10.1039/c8cp06232c.

[33] Schrödinger Release 2018-2: Maestro, Schrödinger, LLC, New York, 2018.

[34] Schrödinger Release 2018-2: LigPrep, Schrödinger, LLC, New York, 2018.

[35] Kaminski GA, Friesner RA, Tirado-Rives J, Jorgensen WL. Evaluation and reparametrization of the OPLS-AA force field for proteins via comparison with accurate quantum chemical calculations on peptides. J Phys Chem B. 2001; 105: 6474. doi: 10.1021/jp003919d.

[36] Schrödinger Release 2018-2: Epik, Schrödinger, LLC, New York, 2018.

[37] Schrödinger Release 2018-2: Glide, Schrödinger, LLC, New York, 2018.

[38] Schrödinger Release 2018-2: Prime, Schrödinger, LLC, New York, 2018.

[39]   Schrödinger Release 2018-2: Field-based QSAR, Schrödinger, LLC, New York, 2018.
[40]   Zheng GX, Xue WW, Wang PP, Yang FY, Li B, Li XF, et al. Exploring the Inhibitory Mechanism of Approved Selective Norepinephrine reuptake inhibitors and reboxetine enantiomers by molecular dynamics study. Sci Rep-Uk. 2016; 6: 26883. doi: 10.1038/Srep26883.